

Broadband TDR Permittivity Spectra of Lossy Soils at Medium to High Water Contents: Separation of Electrode Polarization from Maxwell-Wagner Relaxation by Modeling

Steven Arcone, Steven Grant, Ginger Boitnott
U.S. Army ERDC-CRREL
Hanover, New Hampshire, U.S.A.
Steven.A.Arcone@erdcdren.mil

Abstract—We discuss complex permittivity spectra of two lossy soils measured from 6 kHz to 6 GHz using time domain reflectometry, in which Maxwell-Wagner relaxation (MWR) is present but also unwanted electrode polarization EP, mainly below 1 MHz, is strong. The soils are mostly quartz, with one having lesser calcite and the other lesser gypsum. Volumetric water contents ranged from 8.5–30.9%. We use a simple model that adds an EP diffusion term to Debye-type terms for the MWR and free water relaxation centered near 19 GHz, and which allows us to separate the EP from the MWR. All samples show MWRs centered from 1–196 MHz, regardless of water content, and with small to significant Cole-Cole factors. The increasing water content diminishes the effect of MWR, likely by decreasing the conductive and dielectric contrasts between isolated inclusions and the soil matrix, but still can strongly contribute to attenuation rate across the 100–1000 MHz GPR bandwidth.

Index Terms— dielectric permittivity, electrode polarization, Maxwell-Wagner, soils

I. INTRODUCTION

Maxwell-Wagner interfacial relaxations (MWR, [1]) are generally centered within the 1–20 MHz range of complex relative permittivity spectra, ϵ^* , of moist soils [2, 3]. For fine-grained soils with volumetric water contents less than about 10% MWR can significantly add to attenuation rates within the ground-penetrating radar (GPR) bandwidth of 100–1000 MHz. Modeling of time domain reflectometry (TDR) data [3] shows it to be characterized by a Cole-Cole-type Debye relaxation [4] that extends MWR effects from about 1 GHz to well below 1 MHz. We previously processed TDR data down to 1 MHz [3], where a rise of the real part of ϵ^* (ϵ') suggested electrode polarization (EP) was present and would affect measurements of soils with higher conductivities. Here we test soils for MWR over a wider bandwidth and at higher water contents and conductivities, and where EP becomes significant.

In EP charge builds between sample and sample holder and mainly affects ϵ' . The greater the sample conductivity then, generally, the stronger the effect, both in magnitude and in the highest frequency at which it begins to affect ϵ' . The process might be characterized by a relaxation centered below 10 kHz, as in conductive water [5–6] or clay-mineral rich soils [7, 8], or by an induced polarization process in which ϵ' rises without bound, as in rocks and soils [9]. In either case, for high conductivity EP can overlap MWR. Based on the low frequency behavior of ϵ^* in our data (and those of others) that suggests conduction is a diffusion process, while higher frequency relaxations are a propagation process, we hypothesized that the two processes, along with free water relaxation (FWR), could be combined into a simple additive model for bulk permittivity.

Our objective was to find if MWR was significant at volumetric water contents above about 8% and its effect upon attenuation rates within the GPR 100–1000 MHz bandwidth. We used modeling to separate MWR from EP and FWR within the ϵ^* spectra of two wet and conductive soils, as determined with TDR. Our model combines a diffusion complex conductivity EP term with a CRIM [3] propagation model that adds volumetrically weighted MWR, FWR, and air terms, the weights being determined by the mineral and water volume fractions. We used a least squares matching approach to minimize the errors for ϵ' and ϵ'' . Our companion paper [10] tests one of these soils at low water contents and conductivities, and with less EP, by combining open-ended coaxial and low frequency impedance methods. The results greatly improve our previous results [3] over a far wider frequency range, and require no modeling to identify the relaxation frequencies.

II. TDR METHODS

We recorded the complete time (t) domain reflection sequence, $R(t)$, resulting from a fast rise-time step-like pulse incident upon a dielectric sample within an open-ended (open circuit) coaxial waveguide sample holder. A reference reflection from a “short” (a metal termination at the back of an air-filled-cell), $V(t)$, is also recorded and

serves as the incident waveform. Ultimately, we used the ratio of the reflection coefficients in the frequency (f) domain derived from these two measurements to derive ε^* following the Laplace transform methods described in several references [2, 3, 11–13]. Propagation within the coaxial waveguide and sample are described by $\exp\{i(\omega t - k_0 z)\}$ and $\exp\{i(\omega t - kz)\}$, respectively, where $k_0 = \omega/c$ and z is distance. For this dependency ε' and ε'' are then related to ε^* as

$$\varepsilon^* = \varepsilon' - i\varepsilon'' \quad (1)$$

We used a center conductor pin length, $d = 2.02$ mm, but an effective pin length derived by calibration with known permittivity standards in data reduction. The 15 mm long cell had a 3.69 mm inside diameter and a 1.58 mm outer diameter of the pin. The filled cell provided about 13 mm of sample above the pin. The effective length of the sample cell is, essentially, the effective length of the pin as long as it is well covered by the sample.

We used an Agilent 86100C oscilloscope with a 54754A differential TDS module, and a 40 ps pulse rise time. We recorded reflections lasting from 2.5 ns (0.61 ps sampling rate at 4096 points) to 163.84 μ s (40 ns sampling rate at 4096 points). We averaged 256 waveforms, which increased the signal to noise ratio and reduced variance, primarily caused by time jitter. The 0.61 ps sampling rate gives a Nyquist frequency of 820 GHz; 9.77 ps gives 51 GHz, etc. We merged the reductions of each run into single sets that spanned 6.1 kHz to 10 GHz.

We computed the one-way attenuation rate β (dB m^{-1}) from the imaginary part of the wave number in the exponential propagation term $\exp(-ikz)$, where $z = 1$ m. The expression is

$$\beta = 8.686(\omega/c) \left(\varepsilon'^2 + \varepsilon''^2 \right)^{1/4} \sin \left[\frac{\tan^{-1}(\varepsilon''/\varepsilon')}{2} \right] \quad (2)$$

At frequencies near and below 1 MHz $\varepsilon'' \gg \varepsilon'$ even for mildly conducting samples (< 0.001 S m^{-1}). Therefore, at the lower frequencies the phase term is near unity and the magnitude is dominated by ε'' in equation (2) and so any inflection within the behavior of β indicates relaxation.

III. MODELING

We assume that the spectra of ε^* are determined by a complex conductivity diffusion process superimposed upon wave propagation terms, related to MWR, FWR, and a constant term from the air component. We combined propagation terms using the empirical volumetrically-based complex refractive index ($n^* = \sqrt{\varepsilon^*}$) method (CRIM; [3, 14, 15]), whereby n^* equals the sum of the indices of the constituent components, weighted by their respective volume fractions, v , such that

$$n^* = n_m v_m + n_w v_w + n_a v_a \quad (3)$$

Here m , w , and a stand for mineral, water and air, respectively, and $n_a = 1$. The phase velocity $v_{ph} = c/\text{Real}(n^*)$. We then constructed ε^* by squaring n^* and adding the diffusive complex σ_b^* term such that

$$\varepsilon^* = (n^*)^2 + \varepsilon_\sigma^* \quad (4)$$

in which, following [9], we express the EP contribution as a complex conductivity, ε_σ^* such that

$$\varepsilon_\sigma^* = A/\omega^\eta - j\sigma_b/\omega \varepsilon_0 \quad (5)$$

Here A is the amplitude of the real part, η is the exponential coefficient of frequency, $\varepsilon_0 = 8.854 \times 10^{-12}$ F m^{-1} , and σ_b is the bulk DC conductivity.

In this approach equation (4) allows the contribution of each dielectric and conductive process to the attenuation rate to be approximately calculated. Eq. (5) may not be an accurate representation below 6 kHz but we only require an equation that fits our data and so allows MWR to be separated. The σ_b dominates ε'' when the low-frequency asymptotic behavior of ε'' becomes logarithmically linearly dependent on frequency, and allowed us to use ε'' to first estimate σ_b for our modeling.

CRIM assumes that statistically, each polarizing entity (e.g., a single wet mineral grain) is much less than a wavelength in size [12, 14]. The relaxation parameters derived are effective values that account for molecular scale interactions. The main quantities of interest are f_{rel} , α and β .

We used the Cole-Cole version of the Debye model to define ε_i^* for the MWR and FWR such that

$$\varepsilon_i^* = \varepsilon_{inf} + (\varepsilon_s - \varepsilon_{inf}) / (1 + (j f / f_{rel})^{1-\alpha}), \quad (10)$$

where ε_{inf} is the asymptotic value of ε_i at very high frequency, ε_s is the very low-frequency value, and f is frequency. The quantity α is the Cole-Cole broadening factor, likely caused by multiple close relaxations related to a spread of σ and shape contrasts between soil matrix and inclusions. A small α extends the relaxation bandwidth.

We used the v_m for MWR because its frequency is significantly below that of FWR, which suggests that it does not involve any significant amount of free water but rather, water finely dispersed. We used v_w for the FWR.

We determined our best fits to the data by fixing the water parameters with the values for 25°C, of $\varepsilon_{inf} = 5.2$, $\varepsilon_{st} = 78.34$, $f_{rel} = 19.22$ GHz [16] and $\alpha = 0.00$, and then adjusting S , η , σ_b , ε_{inf} , ε_{st} , f_{rel} and α until the added average rms errors for ε' and ε'' between 6.1 kHz and 2–5 GHz were less than about 10%. We chose these limits to alleviate effects of any errors above 2 or 5 GHz, whichever limit showed the onset of large errors, but either is far above any MWR. We display our model results from 10

Hz to 10 GHz to show the expected data trends. The conductivities of the bulk samples and the added water are too low to require adjusting the free water values for salinity [17].

IV. RESULTS

A. NaCl methanol solution calibration

We used saline methanol with an air reference to validate the TDR results because the strong conductivity produced EP and the f_{rel} at 25° C, near 1 GHz is not significantly affected by salinity [18]. Unfortunately, there are no substances with well documented relaxations below 100 MHz with which to test our interpretative modeling procedure. Fig. 1 shows that the rms error for the real part from 1 MHz to 5 GHz is 1.8%. For the imaginary part the error is less than 1% from 10 MHz to 5 GHz.

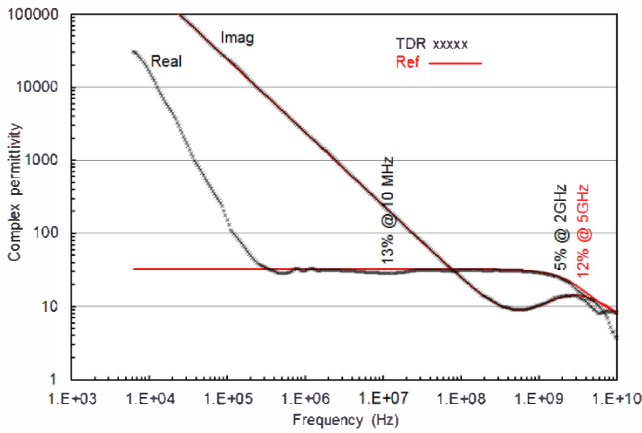


Figure 1. Complex permittivity of saline methanol measured at 0.1348 S m⁻¹, compared with previous measurements [18]. Vertical labels indicate large errors. EP affects ϵ' below 1 MHz. The methanol has relaxations at 3.09, 26.9 and 142 GHz.

B. Quartz-Calcite soil

Our calcitic quartz and feldspar soil is from Yuma, AZ. Particle sizes are < 53 μ . Minerals present and their estimated weight percentages ($\pm 10\%$) obtained by an independent laboratory using XRD and SEM/ED-XRF analysis, are quartz (50%), Calcite (15%), sodium-calcium feldspars (10%), smectite (10%), chlorite-kaolinite (5%) and mica (10%). Although the accuracy is poor quartz is dominant, the quartz and feldspars, which likely contribute no conductive ions, comprise about 60%, and calcite is next most present. For particles < 5 μ quartz and calcite dominate the XRD spectra. SEM images show 1–5 μ size particles clinging to 10–50 μ size quartz particles larger quartz particles. We added doubly distilled and deionized (“milliQ”) water, with $\sigma < 0.00012$ S m⁻¹.

Fig. 2 shows ϵ' , ϵ'' and β at 3 v_w values. The solid black lines are the data and the red dashed lines are the models. The added errors for ϵ' and ϵ'' total less than 9%. All ϵ' sharply rise below 1 MHz with decreasing f because of EP,

which requires extremely high constants for A in eq. (9). Between 1 and 100 MHz the ϵ' slope greatly decreases, which is the region of the MWR. Above 100 MHz ϵ' then decreases slightly and then levels up to several GHz. The ϵ'' and β appear dominated by σ_b but Fig. 3 shows that this is not the case above about 10 MHz.

The bottom row of Fig. 3 details the contributions to the β , while the top row gives details of the MWR models. The contributions are weighted by the v_m for MWR, total volume for conductive, and v_w for water. The conductive contribution uses the real part of n for the propagation terms and the modeled value of σ_b . They don't add exactly to the total β because terms are not linearly combined when computing total β ; but there is less than 3% error by 1 GHz. The MWRs have large α values that enlarge their bandwidths to affect β well above their range of 1–15 MHz. For example, at 8.3% water content the MWR contribution of about 15 dB m⁻¹ at 100 MHz equals the conductive contribution and by 1 GHz the MWR greatly exceeds it. At higher water contents the bulk conductivity increases and so at 15.4% water content the MWR contribution does not equal the conductive one until about 1 GHz. Below 10 MHz the conductive contribution is independent of ϵ' , despite its large EP value. In general, the MWR contribution from 100–1000 MHz for all water contents is similar, significant, but changes in its ratio to conductive losses.

C. Quartz-gypsum soil

We have previously discussed this lossy Iraqi soil [3], but over less bandwidth. XRD analysis found, by weight, gypsum (10%), quartz (80%), unspecified plagioclase feldspars (10%) and insignificant salt or salt elements. SEM micrographs showed significant crystallites, grains and crusts on the quartz. EDA showed calcium, sulfur and oxygen within one crystalline crust and within several small grains attached to the quartz surfaces.

Figs. 4 and 5 show results qualitatively similar to Figs. 2 and 3: large EP effect in ϵ' below 1 MHz, and ϵ'' and β dominated by σ_b below about 10 MHz. Quantitatively, there is a more pronounced MWR effect from 0.1–100 MHz at the lowest water content, as expected, while the MWRs at 17.0 and 33.8% water contents are centered much higher in frequency and have weaker values of ϵ_s and ϵ_{inf} . Consequently, Fig. 5 shows that the MWR contribution to β at 6.2% dominates above 100 MHz, while at 17.0% it does not equal the conductive contribution until about 2 GHz, and at 33.8% the MWR contribution never exceeds about 22 dB m⁻¹ while the conductive contribution levels above 1 GHz at about 260 dB m⁻¹. In addition, we find that α has no value at this high water content.

V. DISCUSSION AND CONCLUSIONS

At v_w less than about 10% MWRs exist in the range of about 1–15 MHz [3], but these measurements were above 1.6 MHz and so did not account for any effects of EP.

Here at 8.3% and 6.2% v_w we find MWR at 3.89 and 2.40 MHz, respectively, accounting for EP. As v_w increases so does σ_b and f_{rel} , reaching 14.33 MHz at 15.4% for the quartz-calcite soil and 35.52 MHz at 17.0% for the quartz-gypsum soil. This trend is consistent with general theory of MWR, such as formulated by Matzler [19] for a spherical conductive inclusion whereby f_{rel} is expressed as

$$f_{rel} = \sigma_2 / 2\pi\epsilon_0(2\epsilon_1' + \epsilon_2'), \quad (10)$$

in which σ_2 is the real conductivity of an inclusion, ϵ_1' is the real part of ϵ_1^* of the host medium, and ϵ_2' is that of the inclusion. Equation (1) differs little from $f_{rel} = 1/2\pi\tau$, where the relaxation time $\tau = \sigma/\epsilon$ is the time needed for a distribution of polarized molecules within a conductive inclusion to return to equilibrium under zero electric field conditions. Matzler considered the conductive inclusions within his quartz soil to be hematite because the gravimetric water content was less than 0.2%. The critical quantity is σ_2 , which could significantly exceed the bulk soil value, σ_b' . As σ_2 increases with increasing v_w , so should f_{rel} .

At saturation this trend does not continue because although it reached as high as 196 MHz at 33.8% v_w for the quartz-gypsum soil, the quartz-calcite soil at 30.8% showed at an extremely low $f_{rel} = 1.28$ MHz. Consequently it is not clear if MWR is the cause of the slight relaxation at the saturation water contents; even though we have water and inclusive minor minerals with contrasting permittivity, f_{rel} dramatically dropped for the quartz-calcite soil. We speculate that the conductivity of the inclusions also dropped but further experimentation is required to find if this behavior can be repeated.

In all cases we conclude that MWR are likely to contribute significantly to attenuation rates at high to saturated water contents, as we found in 3 of our 4 cases. Only the saturated gypsum soil showed a significant decrease in MWR loss and domination by conductive losses up to a few GHz. The reason may be that this soil had no clay mineral detectable by X-ray diffraction.

ACKNOWLEDGEMENTS

This work was supported by the U.S. Army Engineer and Research Development Center 6.1 program in basic research. Permission to publish was granted by the Director, Cold Regions Research and Engineering Laboratory.

REFERENCES

- [1] K. W. Wagner, "Erklärung der dielektrischen nachwirkungsvorgänge auf grund Maxwellscher vorstellungen," *Archiv für Electrotechnik*, vol. 2, pp. 371–387, 1914.
- [2] T. Ishida, T. Makino, and C. Wang, "Dielectric-relaxation spectroscopy of kaolinite, montmorillonite, allophane, and imogolite under moist conditions," *Clays and Clay Minerals*, vol. 48, pp. 75–84, 2000.
- [3] S. A. Arcone, and G. E. Boitnott, "Maxwell-Wagner relaxation in common minerals and a desert soil at low water contents," *J. Applied Geophysics*, vol. 81, pp. 97–105, 2012.
- [4] K. S. Cole, and R. H. Cole, "Dispersion and absorption in dielectrics-I: Alternating current characteristics," *J. Chemical Physics*, vol. 9, pp. 341–352, 1941.
- [5] P. Ben Ishai, Z. Sobol, J. D. Nickels, A. L., and A. P. Sokolov, 2012, "An assessment of comparative methods for approaching electrode polarization in dielectric permittivity measurements," *Rev. Sci. Instr.*, vol. 83, pp. 083118-1 – 083118-8, doi: 10.1063/1.4746992, 2012.
- [6] Y. Feldman, E. Polygalov, I. Ermolina, Y. Plevaya, and B. Tsentsiper, "Electrode polarization correction in time domain dielectric spectroscopy," *Measurements Science and Technology*, vol. 12, pp. 1355–1364, 2001.
- [7] S. A. Arcone, S. A., Grant, S.A., G. Boitnott, and B. Bostick, 2008, "Complex permittivity and clay mineralogy of grain-size fractions in a wet silt soil," *Geophysics*, vol. 73, pp. J1–J13, 2008.
- [8] B. Rotenburg, A. Cadene, J.-F. Dufreche, S. Durand-Vidal, J.-C. Badot, and P. Turq, "An analytical model for probing ion dynamics in clays with broadband dielectric spectroscopy," *J. Physical Chemistry*, vol. B109, pp. 15548–15557, 2005.
- [9] H. J. Vinegar, and M. H. Waxman, "Induced polarization of shaly sands," *Geophysics*, vol. 49, pp. 1267–1287, 1984.
- [10] S. A. Grant, S. A. Arcone, and G. E. Boitnott, "Maxwell-Wagner-Sillars, adsorbed water, and free-water dielectric relaxations within a hydrated arid-zone calcic soil," in *Proceedings of 15th International Conference on Ground-Penetrating Radar*.
- [11] R. H. Cole, J. G. Berberian, S. Mashimo, G. Chrysikos, and A. Burns, "Time domain reflection methods for dielectric measurements," *J. Applied Physics*, vol. 66, pp. 793–802, 1989.
- [12] J. G. Berberian, and E. King, "An overview of time domain spectroscopy," *J. Non-crystalline solids*, vol. 305, pp. 10–18, 2002.
- [13] S. Mashimo, T. Umchara, T. Ota, S. Kuwabara, N. Shinyashiki, and S. Yaiharu, "Evaluation of complex permittivity of aqueous solution by time domain reflectometry," *J. Molecular Liquids*, vol. 36, pp. 135–151, 1987.
- [14] A. M. Shutko, and E. M. Reutov, "Mixture formulas applied in estimation of dielectric and radiative characteristics of soils and grounds at microwave frequencies," *IEEE Trans. Geoscience and Rem. Sens.*, vol. GE-20, pp. 29–32, 1982.
- [15] C. Birchak, G. Gardner, J. E. Hipp, and J. M. Victor, "High dielectric constant microwave probes for sensing soil moisture," *Proc. IEEE*, vol. 62, pp. 93–98, 1974.
- [16] Kaatze U., "Permittivity of pure water, at standard atmospheric pressure, over the frequency range 0–25 THz and the temperature range 0–100° C," *J. Physical Chemistry Reference Data*, vol. 36, pp. 1–18, 2007.
- [17] D. H. Gadani, V. A. Rana, S. P. Bhatnagar, A. N. Prajapati, and A. D. Vyas, "Effect of salinity on the dielectric properties of water," *Indian J. Pure and Appl. Phys.*, 50, 405–410, 2012.
- [18] J. Barthel, R. Buchner, and M. Munsterer, "Dielectric properties of nonaqueous electrolyte solutions, Part 2a," in *Electrolyte data collection*, J. Barthel, R. Neueder, eds, Frankfurt am Main, DEHEMA, Deutsche Gesellschaft für Chemisches, 1996.
- [19] C. Matzler, "Microwave permittivity of dry sand," *IEEE Trans. Geoscience Rem. Sens.*, vol. 36, pp. 317–319, 1998.

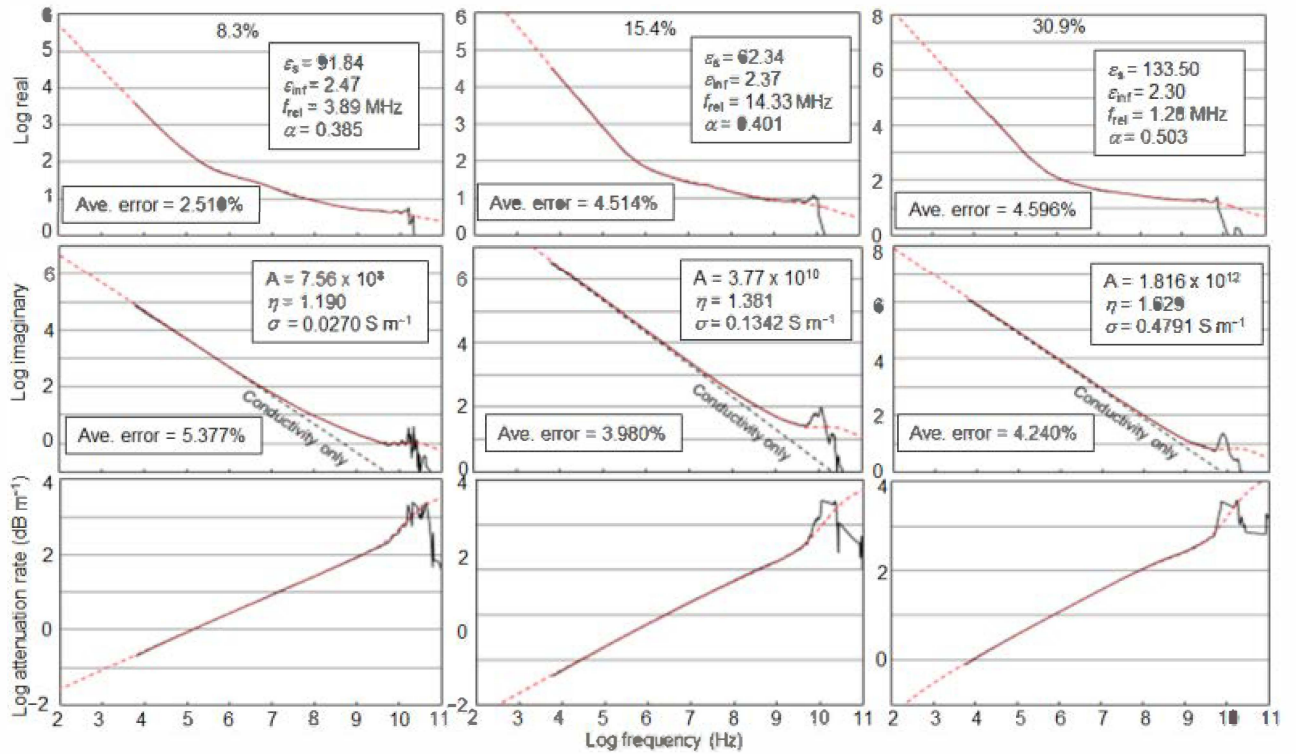


Fig. 2. MWR spectra (top row) and detail of the attenuation rates (bottom row) for the Yuma, AZ soil at 3 volumetric water contents, matching models (red dashed lines) and behavior of imaginary parts for conductivity only (black dashed lines). MWR parameters are in the boxes within the real parts graphs and the complex conductivity parameters are in those for the imaginary parts.

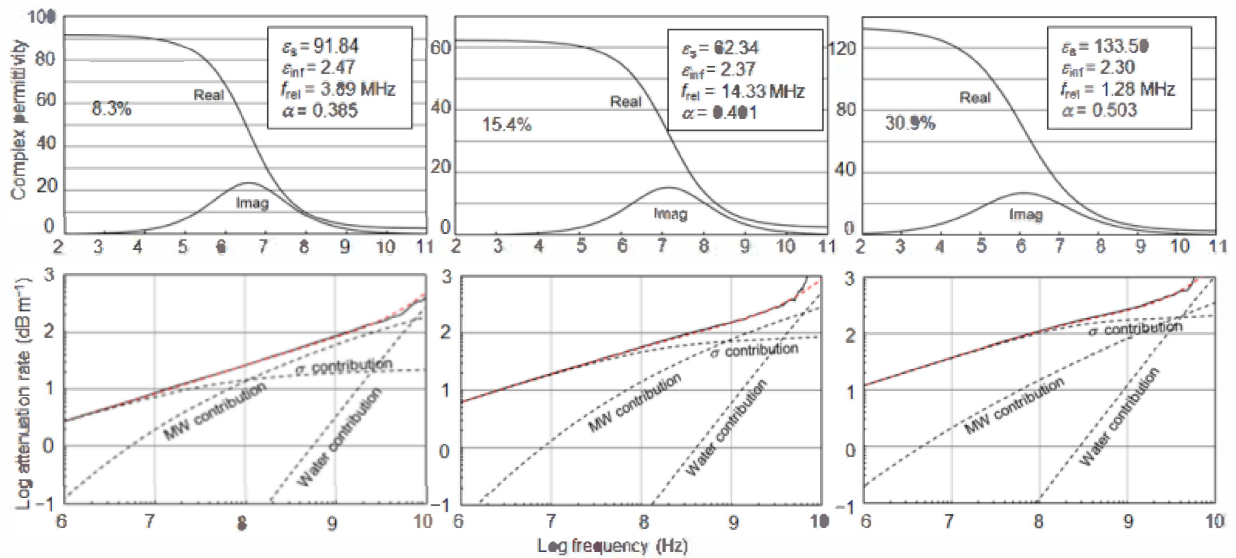


Fig. 3. MWR component spectra (top row) and detail of the attenuation rates (bottom row) for the Yuma soils. In the lower row the solid lines are the data and red dashed lines are the matching models. The black dashed lines show the contributions of the complex conductivity, MWR and FWR. Within the typical GPR bandwidth of 100–1000 MHz, the MWR attenuation rate appears similar for all water contents; e.g., at 100 MHz it is about 15 dB m⁻¹ and then increases to about 70 and more. However, it equals or exceeds the conductive contribution at the lowest water content, is less than or equal to it at the medium water content, and far below it at the highest water content.

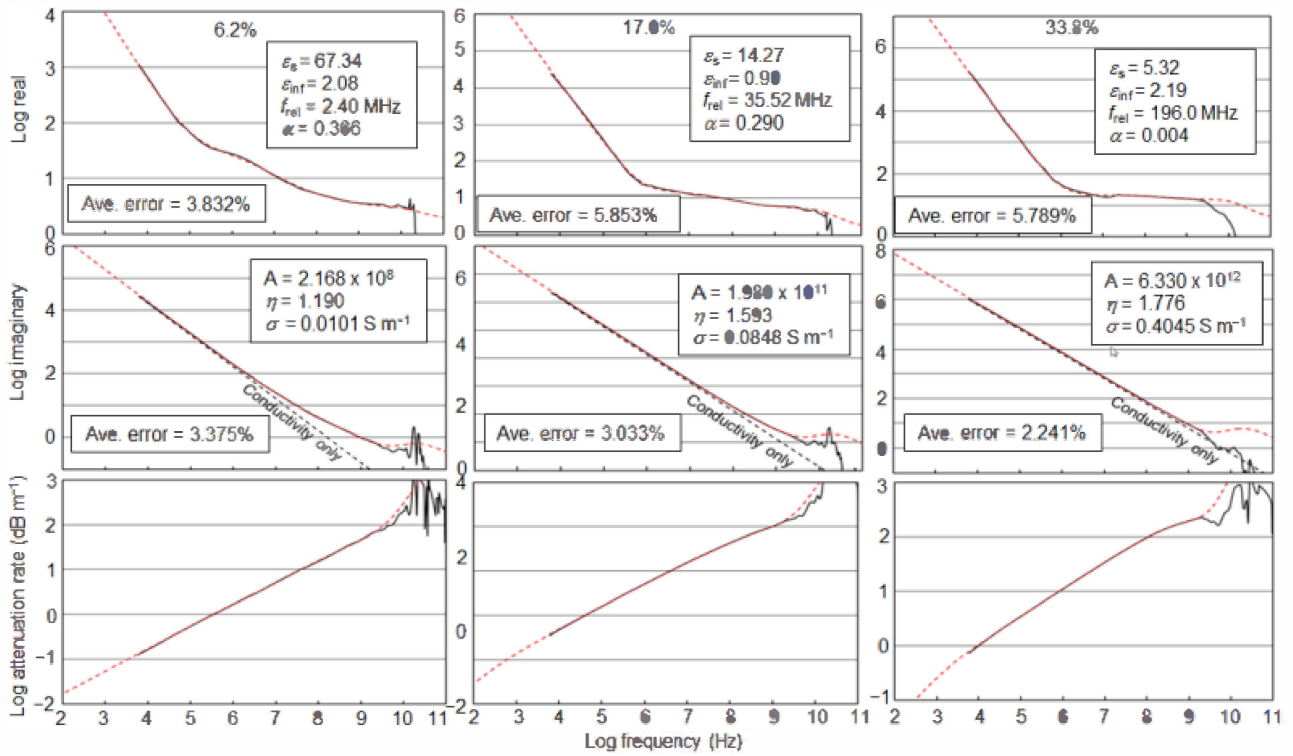


Figure 4. MWR spectra (top row) and detail of the attenuation rates (bottom row) for the Iraq soil at 3 volumetric water contents, matching models (red dashed lines) and behavior of imaginary parts for conductivity only (black dashed lines). MWR parameters are in the boxes within the real parts graphs and the complex conductivity parameters are in those for the imaginary parts.

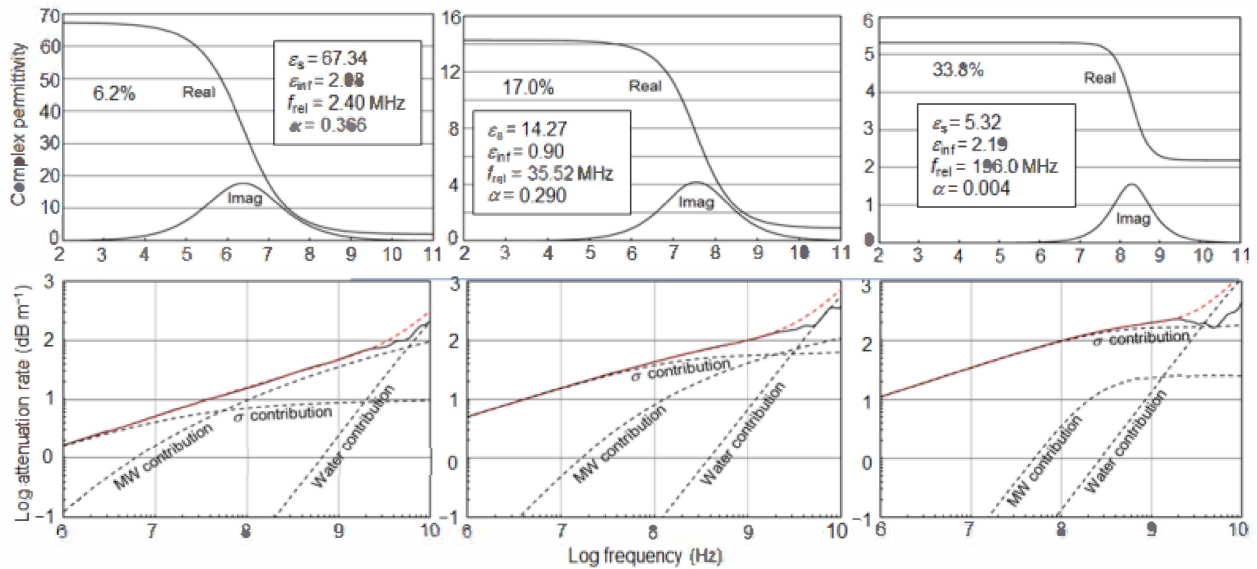


Figure 5. MWR component spectra (top row) and detail of the attenuation rates (bottom row) for the Iraq soil at 3 volumetric water contents. In the lower row the solid lines are the data and red dashed lines are the matching models. The black dashed lines show the contributions of the complex conductivity, MWR and FWR. Within the typical GPR bandwidth of 100–1000 MHz, the MWR attenuation rate equals or greatly exceeds the conductive contribution at the lowest water content, is less than it at the medium water content, and far below it at the highest water content.